



Influence of environmental parameters on workers' dust inhalation in underground mines

Rongting Huang¹ · Wanyi Chen¹ · Yichun Tao¹ · Shilong Yuan² · Fan Geng^{1,2} · Shihang Li^{1,3}

Received: 8 June 2023 / Accepted: 27 December 2023 / Published online: 6 January 2024
© The Author(s), under exclusive licence to Springer-Verlag GmbH Germany, part of Springer Nature 2024

Abstract

Much dust is generated in underground coal mining processes, posing threats to workers' health and safety production. Dust enters the human body mainly through inhalation, primarily determined by the dust concentration around workers. In this study, the airflow field and dust distribution in the tunnel are simulated with FLUENT software. The breathing zone for a worker was defined to clarify the extent of external dust distribution influencing dust inhalation. The effects of human respiration, dust production rates, air supply velocities, and workers' positions on dust concentration in the breathing zone were investigated. The results show that there is upward airflow around the worker standing in the center of the air circulation. Human breath barely influences the airflow distribution and respirable dust concentrations in the breathing zone. Reducing the dust production rate in the tunnel can decrease the respirable dust concentration in the breathing zone by almost the same proportion. While increasing the air supply velocity by 50% would reduce only 20% of dust in the breathing zone. The dust concentrations vary along the roadway, in which the low concentration zone is located in the middle, more than 1.0 m away from the dust-producing surface and the wind surface. The research contributes to reducing workers' dust exposure with suggestions regarding ventilation optimization and working position selection.

Keywords Respirable dust · Breathing zone · Human respiration · Underground environmental parameters · Numerical simulation

Introduction

Despite China's commitment to reach a CO₂ emission peak by 2030 and achieve carbon neutrality by 2060, coal remains the dominant energy resource in the country. A large amount of dust is inevitably generated during coal mining (Zhang et al.

2021; Paluchamy et al. 2021), posing health risks to workers (Jiang et al. 2021). Ventilation can dilute and remove dust particles in mine tunnels, but it cannot cover every corner effectively in practice (Liu et al. 2019; Gui et al. 2020; Wang et al. 2020). The dust concentrations in some local underground environments are still high, ranging from 1200 to 8000 mg/m³ (Li et al. 2019; Yin et al. 2019), which significantly exceeds the maximum allowable concentration stipulated in the "Coal Mine Safety Regulations of China (2022)." Prolonged exposure to dust can cause chronic inflammation and pulmonary fibrosis in the lungs, resulting in pneumoconiosis (Trechera et al. 2022; Shekarian et al. 2021). It is closely associated with respirable dust, which has an aerodynamic diameter of less than 7.07 μm and can penetrate and accumulate in the lung tissues (Zhao 2023). Coal workers' pneumoconiosis accounts for over 50% of annual officially reported occupational cases in China (Chen et al. 2022a, b). Respirable dust can cause irreversible damage to human lungs. Hence, it is imperative to find effective dust removal methods to protect workers from occupational hazards (Hu et al. 2021). A critical step in this process is to study the exposure characteristics of respirable dust for mine workers.

Responsible Editor: Shimin Liu

✉ Rongting Huang
huangrongting@cumt.edu.cn

- ¹ Jiangsu Engineering Research Center of Dust Control and Occupational Protection, School of Safety Engineering, China University of Mining and Technology, Xuzhou 221116, China
- ² School of Low-Carbon Energy and Power Engineering, China University of Mining and Technology, Xuzhou 221116, China
- ³ Jiangsu Key Laboratory of Coal-Based Greenhouse Gas Control and Utilization, Carbon Neutrality Institute, China University of Mining and Technology, Xuzhou 221116, China

Numerous studies have investigated dust distribution patterns in underground tunnels. Chen et al. (2022a, b) simulated the spatial and temporal evolution of dust and suggested that the dust concentration in the footway and transport route generally exhibited a rapid increase and a gradual decrease from the heading face. Wang et al. (2015) performed a numerical simulation and found that the dust concentration declined sharply from the heading face and then slowly decreased under a high dust production rate. Yao et al. (2020) conducted a field measurement and observed that from the heading face to the exit of the tunneling roadway, the dust concentration fluctuated around a constant value and gradually diminished. These studies indicated that dust and respirable dust were not uniformly distributed in the roadway. Therefore, the research on the dust exposure of mine workers should focus on the workers' surrounding space that covers their respiration.

To limit the research zone for workers' dust respiration, the breathing zone was commonly defined as the area within a radius of 0.30 m (or 10 in) of the human nose and mouth (Ojima 2012). Guffey et al. (2001) sampled different parts of the human body model in a wind tunnel and discovered that gas distribution near the human body had significant spatial differences. Lidén and Waher (2010) suggested that for workers exposed to large particles, the radius of their breathing zone should be reduced to 0.10 m. Ojima's study (2012) recommended that the definition of the breathing zone of workers handling organic solvents should be decreased to 0.05–0.10 m. These studies indicated that a smaller breathing zone had a gas or particle concentration closer to the human inhalation concentration. Consequently, the breathing zone was redefined in the present work as the hemispherical space around the human face, with a radius of 0.20 m and the center between the nostrils.

The dust concentration in the breathing zone within complex underground tunnels is susceptible to external environmental factors. In such cases, the individual sampling methods can only obtain average dust concentration in the breathing zone but lack detailed real-time dust distribution and variations, particularly concerning human respiration processes. In contrast, the numerical simulation methods are reliable for obtaining detailed data on a small scale and have found widespread application in various studies. Some researchers have utilized simulations to identify breathing zones with varying dust concentrations in different regions. For instance, Lu et al. (2021) simulated the dust concentration in workers' potential breathing zones at different breathing height levels to delineate the dust safety zone for workers at different stations in the longwall mining face. Xie et al. (2021) simulated the airflow field and dust distribution after tunnel blasting, revealing more severe dust pollution at the 3.00 m personnel breathing zone than at other heights ahead of the driving face. Zhou et al. (2022) simulated the dust distribution in a fully mechanized mining face under various inclination angles and established the functional relationship between the dust concentration in the sidewalk breathing zone and the distance from

the working surface. Numerical simulations were also employed to explore strategies for minimizing dust concentrations in the breathing zone. Alshitawi et al. (2019) designed a personalized air curtain through numerical simulation to maintain the air quality in the human breathing zone and determined an optimal airflow velocity. Cai et al. (2019) simulated the coal dust distribution at different airflow velocities to determine the best airflow velocity for lower dust concentrations in the footway breathing zone. They found higher dust concentrations at breathing heights along the coal transportation route than on the footway.

While these studies have contributed extensive data to the breathing zone research, variations in respirable dust influenced by external dust-containing airflow and associated parameters have been insufficiently discussed. Therefore, this study employed a coupled computational fluid dynamics (CFD) and discrete phase model (DPM) approach to simulate the airflow and dust distribution in the breathing zone of underground workers, considering the gas–solid two-phase flow. The study comprehensively examined the effects of large-scale external environmental parameters, aiming to provide fundamental research data and theoretical guidance for preventing dust-related occupational diseases among underground workers.

Model establishment and simulation parameters

Mathematical model

The CFD-DPM method was adopted to simulate the movement of airflow and dust in underground tunnels. The airflow, regarded as the continuous phase, was solved using the Eulerian method with the realizable k - ϵ model. The dust particle trajectories, regarded as the discrete phase, were tracked using the Lagrangian method by integrating the forces acting on each particle (Song et al. 2021).

The following assumptions were made for the simulation:

- (1) The airflow in the roadway was assumed to be an ideal incompressible fluid.
- (2) The airflow field was assumed to be isothermal, with the omission of heat transfer considerations during computation.
- (3) The shape details of the dust were omitted, and the dust was approximated as regular spherical particles.
- (4) The interaction between dust particles was disregarded.

Mathematical model of airflow

Airflow movement conforms to the continuum equation and Navier–Stokes equation are as follows (Lu et al. 2021):

$$\frac{\partial(\rho u)}{\partial x} + \frac{\partial(\rho v)}{\partial y} + \frac{\partial(\rho w)}{\partial z} = -\frac{\partial \rho}{\partial t} \tag{1}$$

$$\rho \left(\frac{\partial U}{\partial t} + U \cdot \nabla U \right) = -\nabla p + \mu \nabla^2 U + F \tag{2}$$

The *k*-equation and ϵ -equation in the realizable *k*- ϵ model can be expressed as (Zhou et al. 2022)

$$\frac{\partial(\rho k)}{\partial t} + \frac{\partial(\rho k u_j)}{\partial x_j} = \frac{\partial}{\partial x_j} \left[\left(\mu + \frac{\mu_t}{\sigma_k} \right) \frac{\partial k}{\partial x_j} \right] + G_k - \rho \epsilon \tag{3}$$

$$\frac{\partial(\rho \epsilon)}{\partial t} + \frac{\partial(\rho \epsilon u_j)}{\partial x_j} = \frac{\partial}{\partial x_j} \left[\left(\mu + \frac{\mu_t}{\sigma_\epsilon} \right) \frac{\partial \epsilon}{\partial x_j} \right] + \rho C_1 S \epsilon - \rho C_2 \frac{\epsilon^2}{k + \sqrt{v \epsilon}} \tag{4}$$

where G_k is the generation term of turbulence kinetic energy due to the mean velocity gradient, $G_k = u_t E^2$; $C_1 = \max \left[0.43, \frac{\eta}{\eta + 5} \right]$, $\eta = S_\epsilon^k$; σ_k and σ_ϵ are the turbulent Prandtl special of *k*-equation and ϵ -equation. In FLUENT software, $C_2, C_{1\epsilon}, \sigma_k$, and σ_ϵ are constants with values of $C_2 = 1.9, \sigma_k = 1.0, \sigma_\epsilon = 1.2$.

Mathematical model of dust

The force balance of individual dust particles was expressed as follows (Hu et al. 2020; Geng et al. 2018):

$$m_p \frac{du_p}{dt} = F_D + F_g + F_x \tag{5}$$

where m_p is the particle mass (kg); u_p is the particle velocity (m/s); F_g is the gravitational force on the particle (N); F_x are the additional forces other than drag force, gravity, and buoyancy, such as virtual mass force and thermophoresis force, with the unit of Newton (N); and F_D is the drag force (N) on the particle, which was expressed as (Mo et al. 2020)

$$F_D = \frac{1}{8} \pi d_p^2 C_D \rho \left| u - u_p \right| (u - u_p) \tag{6}$$

where u is the continuous phase velocity (m/s); ρ denotes the continuous phase density (kg/m³); d_p represents the particle diameter (m); and C_D is the dimensionless drag coefficient.

F_x in Eq. (5) consists mainly of the virtual mass force and the thermophoretic force. The virtual mass force of the dust particles in motion was neglected in this study due to their negligible acceleration. The thermophoresis force was also omitted because the external flow field predominantly governed the dust motion. Therefore, F_x was neglected in calculation.

Physical model and grid independence verification

To examine the dust distribution characteristics in the breathing zone, three-dimensional models of the roadway and the worker were constructed based on the actual dimensions. Figure 1 depicts the roadway model as a cube with a standing manikin inside facing the dust-producing surface. The manikin had asymmetrical arms, and the other details of the human body were simplified. Figure 2 illustrates the details of the head of the manikin, and Table 1 presents the geometric parameters of the cube and the manikin.

The grids of 330 K, 360 K, 380 K, 410 K, and 480 K quantities were divided and given the same boundary conditions for the simulations. The total mass flow rate at the two nostrils of

Fig. 1 Structure of the physical model. **a** Overall. **b** Manikin

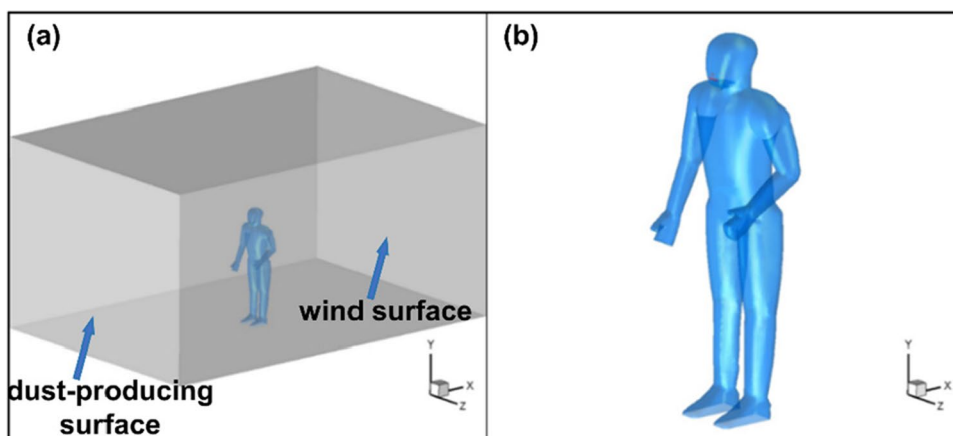


Fig. 2 Partial schematic diagram of a manikin

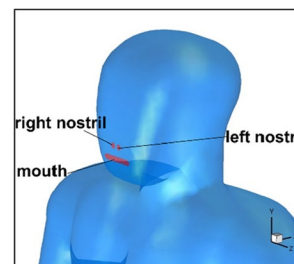


Table 1 Geometric parameters of the physical model

Items	Numerical values
Roadway geometry parameters (m)	6.00×4.00×3.00
Distance between the manikin and the dust-producing surface (m)	3.00
Manikin height (m)	1.80
Diameter of left nostril (m)	0.01
Diameter of right nostril (m)	0.01
Distance between corners of mouth (m)	0.065
Length of both lips (m)	0.055
Width of mouth (m)	0.01

the manikin was then counted. When the number of grids was greater than 360 K, the total mass flow rate fluctuated very gently with the increase in the grid number (Fig. 3). To ensure calculation accuracy and obtain higher calculation efficiency in subsequent calculations, the grid number of 380 K was selected.

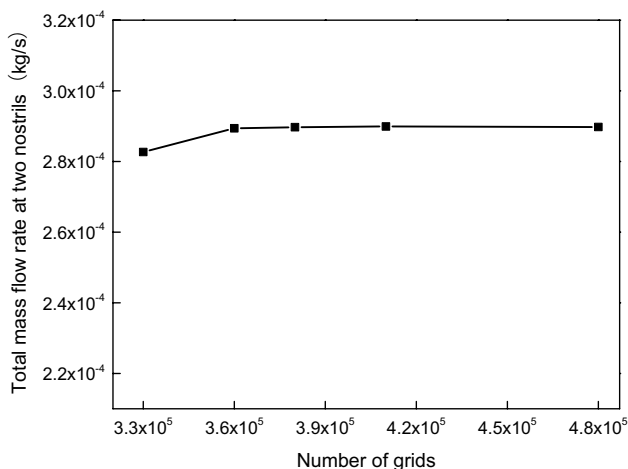
User-defined function and program

The user-defined function (UDF) was employed in FLUENT software based on the human respiratory periodic flow to examine the effect of the human respiratory on the respirable dust concentration in the breathing zone. The basic function structure of the respiratory flow can be expressed as follows (Zhu et al. 2022; Gupta et al. 2011):

$$v = 3\sin(2\pi/3t) \quad (7)$$

where v is the airflow velocity at the nostrils (m/s) and t represents the time (s).

Previous studies have indicated that the maximum instantaneous velocity at the nostrils during human breathing was

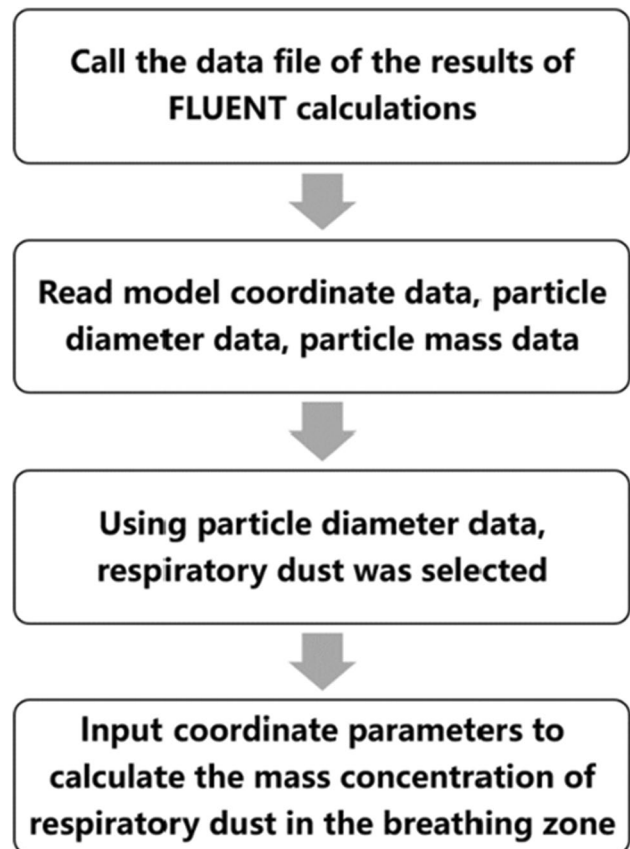
**Fig. 3** Grid independence verification

about 3.0 m/s (Gupta et al. 2011), and the breathing frequency was 12–20 times/min (Zhu et al. 2022). This work focused on the dust-exposed workers in coal mines, who had a relatively higher work intensity. Therefore, the respiratory rate in the human circulatory respiration function was 20 times/min, and the cycle was 3.00 s.

A post-processing program, Post, was written in Visual Basic language to extract data from the simulation results for better post-processing. Post can obtain data from FLUENT calculations, reorganize data to focus on our interest, perform necessary calculations on demand, and display final results with data and plots. The respirable dust data in the following sections were obtained using Post, with the working principles shown in Fig. 4. Post first collects data from FLUENT calculations, filters out particles larger than respirable dust, and calculates mass concentrations based on dust numbers and corresponding particle sizes.

Boundary conditions and parameter settings

In the three-dimensional model of the roadway, the dust-producing surface and the wind surface of the roadway were subdivided into nine equal-area sections. As shown in Fig. 5, fresh

**Fig. 4** Schematic diagram of Post

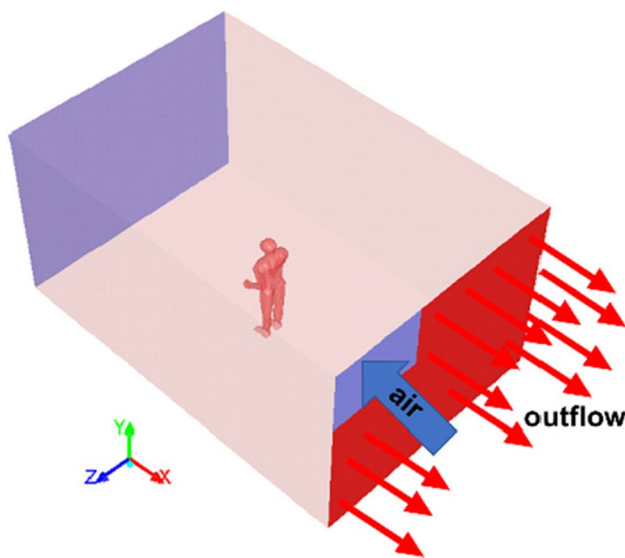


Fig. 5 Diagram of boundary condition settings

air entered the studied roadway from the upper left section of the wind surface, and left from the other sections. The dust was produced uniformly from all nine sections at a constant rate on the dust-producing surface. The control variates method was used to examine the effects of parameters on respirable dust concentration. A control condition with specific simulation parameters and boundary conditions was established, as shown in Tables 2 and 3. The transient pressure-based solver was used in FLUENT software. Computation was conducted using the SIMPLE algorithm. The realizable $k-\epsilon$ model and DPM model were used for turbulence calculation and dust field solution, respectively. In the simulation, the airflow in the tunnel was treated as an incompressible fluid, and heat transfer was ignored. The temperature was left unspecified as the energy equation was turned off in FLUENT in accordance with the isothermal assumption. The inlet and the outlet were set to velocity-inlet and outflow. The validity of the model and parameter settings has been verified in our previous research work (Geng et al. 2018; Gui et al. 2022).

Table 2 Boundary conditions

Items	Boundary conditions/DPM boundaries
Air-inlet section	Velocity-inlet/escape
Other sections of the wind surface	Outflow/escape
Left and right nostrils	Velocity-inlet/escape
Dust-producing surface	Dust produced on the whole surface
Mine roadway walls	Reflect
Worker surfaces	Reflect

Table 3 Parameter settings

Items	Numerical values
Maximum nostril airflow velocity (m/s)	3.0
Breathing rate (times/min)	20
Dust production rate (M) (kg/s)	0.05
Dust particle size distribution (m)	1.00×10^{-6} – 2.00×10^{-4}
Average dust particle size (m)	1.00×10^{-4}
Air supply velocity (V) (m/s)	5.0
Air density (kg/m ³)	1.225
Air viscosity (kg/(m•s))	1.79×10^{-5}

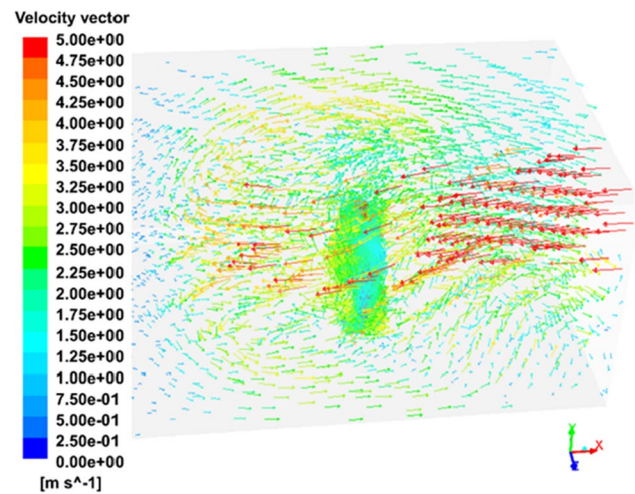


Fig. 6 Airflow vector distribution in the roadway

Results and discussion

Airflow field around a worker

The airflow in the roadway, as the carrier of the dust movement, significantly affects the diffusion and distribution characteristics of the dust. Figure 6 shows the overall airflow vector diagram in the studied roadway under the control condition. The air supply enters the studied roadway at a speed of 5.0 m/s. With increasing distance, part of the airflow starts to deflect downward but generally moves toward the dust-producing surface. Then, the airflow changes direction due to the obstruction of the dust-producing surface and exits the studied roadway from the return side, forming a circulation in the roadway. The worker in the middle of the circulation is exposed to airflow with a high velocity.

To analyze the airflow distribution around the worker, the airflow field near the worker is examined in the $x-z$, $x-y$, and $y-z$ planes, as depicted in Fig. 7. In the $x-z$ plane at the breathing height, part of the airflow on the return side is deflected to the air-inlet side by the entrainment of air

supply with a high velocity. However, the obstruction of the worker prevents airflow from being entrained and creates a more complex flow field near the worker. The worker experiences upward airflow along its surface due to the air vortices formed in front of and behind it ($x = 2.93$ and 3.33 m), as shown in the x - y and the y - z planes.

The air supply affects the airflow field and the elimination of suspended dust in the roadway. The air supply velocity was increased to 10.0 m/s to explore its effect on airflow and dust. Figure 8 compares the roadway airflow at different air supply velocities. The result shows that increasing the air supply velocity enlarges the circulation zone created by the air supply, enhancing the overall airflow velocity in the roadway, and complicates the airflow field around the human body.

The airflow diverges outward when it passes through the dust-producing surface, forming a circulation in the roadway. Moreover, increasing the air supply velocity enlarges the circulation zone. The air supply with a high velocity

entrains part of the airflow on the return side to form circulation. The workers standing in the center of the circulation can cause obstacles to the airflow, creating air vortices before and after their position.

Influence of human respiration on breathing zone characteristics

Influence of human respiration on airflow field

Figure 9 illustrates the distribution of the airflow field in the breathing zone at various time points within a stable breathing cycle. The airflow in the breathing zone primarily ascends along the worker surface (as indicated by the red arrow), except for the airflow near the nostrils that reverses direction when inhalation switches to exhalation. $T = 15.30$ s, 15.75 s, and 16.20 s represent three different time points during the worker's inhalation process. $T = 16.80$ s, 17.25 s, and 17.60 s represent three different time points in a worker's

Fig. 7 Airflow vectors around the worker in different planes

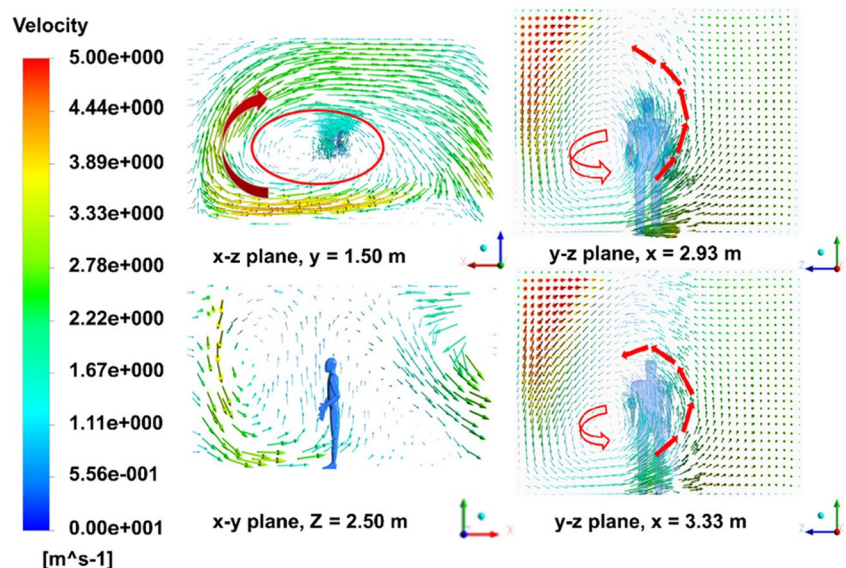


Fig. 8 Airflow traces under different airflow velocities

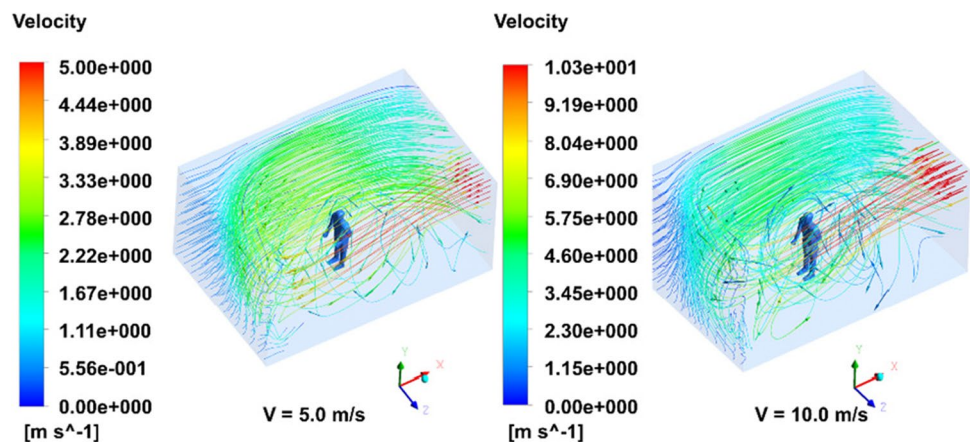
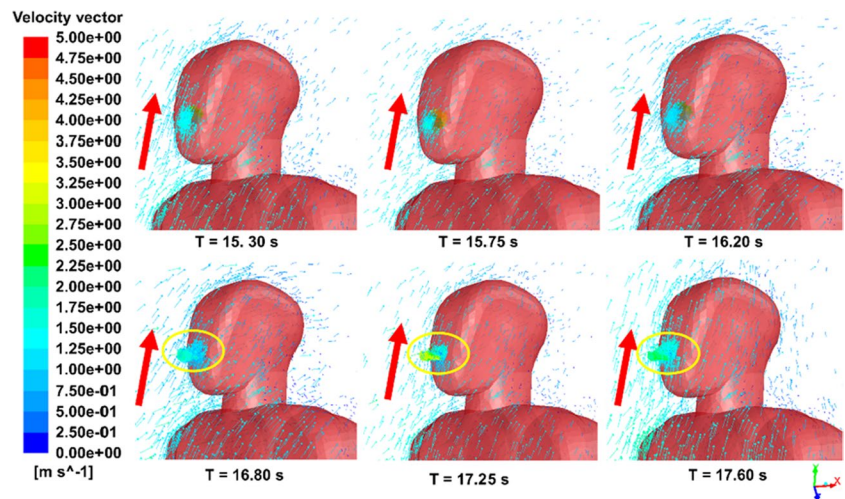


Fig. 9 Airflow vectors at different times in a complete breathing cycle



exhalation process. The worker’s respiration creates a low-pressure field that attracts airflow around the nostrils, resulting in a more drastic change in velocity. $T = 15.75$ and 17.25 s represent the peak velocity moments of inspiration and expiration, respectively. These two moments produce the most substantial entrainment effect, resulting in a more concentrated airflow near the nostrils than at other time points. However, the entrainment is weak and confined to the vicinity of the nostrils, having little effect on the other more extensive areas of the breathing zone.

Figure 10 shows the effect of air supply velocity on the airflow field in the breathing zone. The air supply velocity is initially 5.0 m/s. When it rises to 10 m/s, the airflow velocity in the breathing zone increases by about 50%. However, the airflow distribution remains consistent with that under the control condition. The breathing process only alters the airflow direction near the nostrils at different air velocities and barely affects the overall airflow field in the breathing zone. Therefore, the entrainment brought by human breath can be ignored at the scale of the breathing zone.

Influence of human respiration on dust field

The data on the respirable dust distribution were collected when the dust field was relatively stable. The average respirable dust concentrations within the breathing zone for two complete breathing cycles are computed and presented in Fig. 11. The results show that the respirable dust concentrations in the two cycles are highly consistent: the concentration decreases during inhalation and increases during exhalation. The respirable dust concentration rises gradually during exhalation, probably because the dust in the external ambient airflow promptly replenishes the dust in the breathing zone.

Table 4 reports the results of the independent samples *t*-test that was conducted to examine the effect of

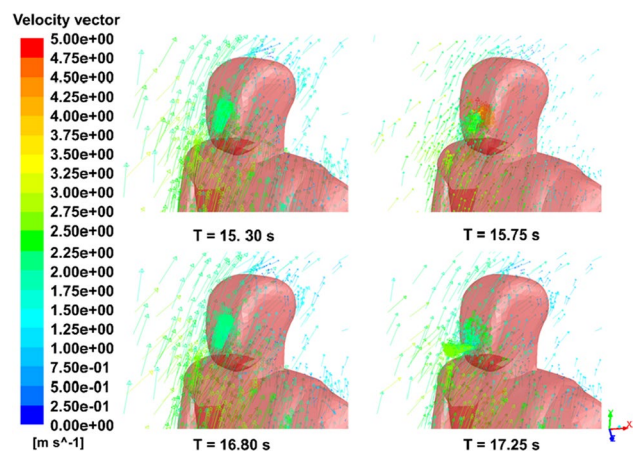


Fig. 10 Airflow distribution in the breathing zone at 10 m/s air supply velocity

the respiratory process on the respirable dust concentration in the breathing zone. The significance values for the 18.00–21.00 s and the 21.00–24.00 s respiratory cycles were both greater than 0.05, indicating no significant difference between the dust concentrations during inhalation and exhalation. Therefore, the influence of human respiratory processes on dust concentrations within the breathing zone can be neglected.

Influence of environmental parameter changes on respirable dust concentration

Influence of dust production rate

The dust production rates were adjusted to 0.10 and 0.01 kg/s, respectively. Figure 12 compares the dust distribution at the same time points but different dust production rates. The airflow turbulence prevents the dust

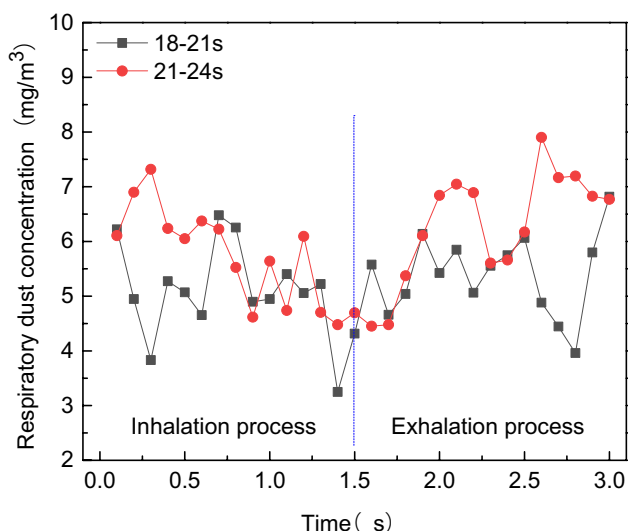


Fig. 11 Respirable dust concentrations in the breathing zone in two complete breathing cycles

Table 4 Respirable dust concentration comparison

Groups		Average value (mg/m ³)	T	Significance
18.00–21.00 s	Inhalation process	5.05	-1.18	0.248
	Exhalation process	5.40		
21.00–24.00 s	Inhalation process	5.71	-1.68	0.104
	Exhalation process	6.30		

stratification in the roadway from being evident. The dust accumulates more at the bottom of the return side than at the air-inlet side at all three dust production rates. This phenomenon is related to two factors: the airflow distribution and the dust-moving path. The airflow initially moves along the inlet side toward the dust-producing surface and is blocked, which changes direction and flows to the return side. During this process, the dust produced from the surface is primarily carried by the airflow to the return side instead of to the inlet side. Also, the airflow velocity decreases due to kinetic energy consumption. Therefore, the airflow on the return side is less capable of entraining dust, leaving more dust deposited on the ground of the return side. Moreover, a small amount of dust accumulates behind the worker because the airflow on the return side disperses near the wind surface. The dust deposited at the bottom of the roadway decreases significantly with the reduction of the dust production rate. Therefore, reducing

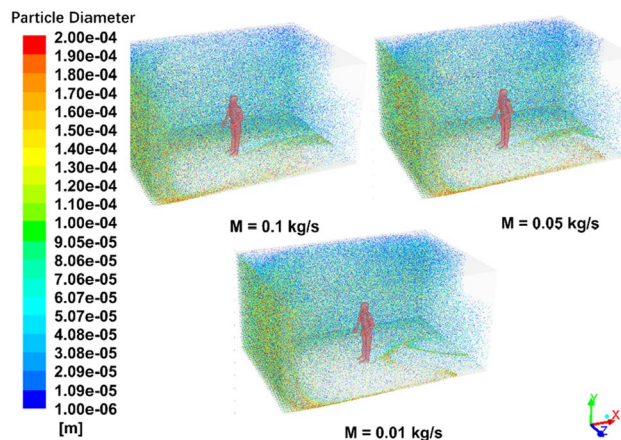


Fig. 12 Spatial and temporal distribution of dust under different dust production rates

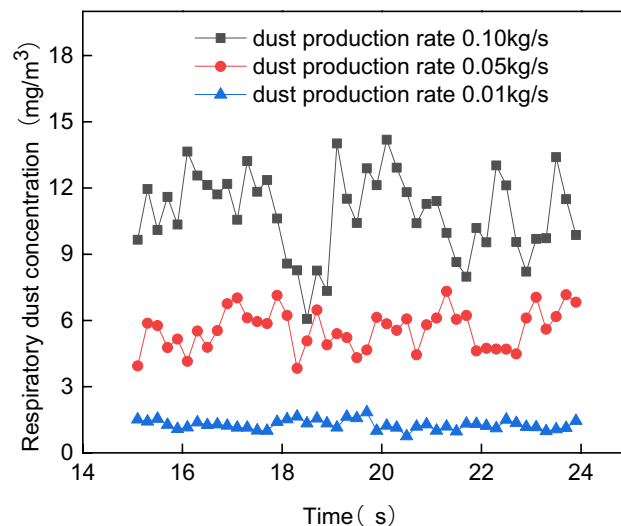


Fig. 13 Respirable dust concentrations in breathing zone under different dust production rates

the dust production rate will directly result in dust reduction in the roadway.

Post was used to extract the numerical values of the respirable dust concentration in the breathing zone over three consecutive cycles with different dust production rates. As shown in Fig. 13, the respirable dust concentration in the breathing zone decreases by approximately 50% when the dust production rate is halved from 0.10 to 0.05 kg/s. The respirable dust concentration in the breathing zone decreases by about 80% when the dust production rate is reduced from 0.05 to 0.01 kg/s. These results indicate that the respirable dust concentration is almost proportional to the dust production rate. Therefore, reducing dust production at the source is an effective way to lower the respirable dust concentration in the breathing zone.

Influence of air supply velocity

Figure 14 compares the spatial and temporal distribution of dust in the roadway before and after increasing the air supply velocity. At the same time ($T=3.00$ s), the newly produced dust in the $V=5.0$ m/s condition has not yet filled half of the tunnel, while in the $V=10.0$ m/s condition, the dust has filled the entire space, with some dust even been carried away from the studied roadway by the wind. That means the dust in the tunnel will be cleaned faster under higher air supply velocity conditions. On the assumption that dust is continuously generated at a certain rate, the existing dust in the tunnel would have a lower concentration under a higher air supply velocity condition than under a lower air supply velocity condition, which can also be seen in Fig. 14 when $T=10.00$ s. So generally, the dust concentration in the studied roadway decreases as the air supply velocity increases.

Figure 15 shows the numerical values of the respirable dust concentrations in the breathing zone under different air supply velocities. The respirable dust concentration in the breathing zone oscillates around 6.00 mg/m^3 when the air supply velocity is 5.0 m/s. The respirable dust concentration in the breathing zone oscillates around 4.00 mg/m^3 when the air supply velocity is 10.0 m/s. This result suggests that increasing the air supply velocity by 50% can lower the dust concentration in the roadway by approximately 20%. Although this dust reduction efficiency is relatively lower than that of reducing the dust production rate, it is still a very effective method for dust reduction due to its easy operation in practice.

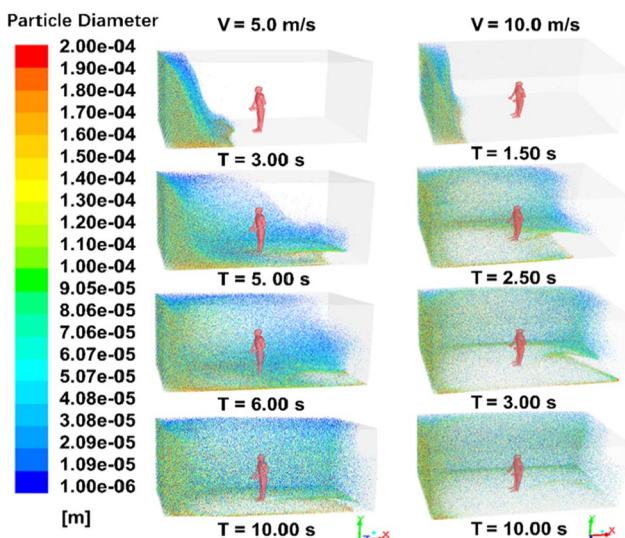


Fig. 14 Spatial and temporal distribution of dust under different air-flow velocities

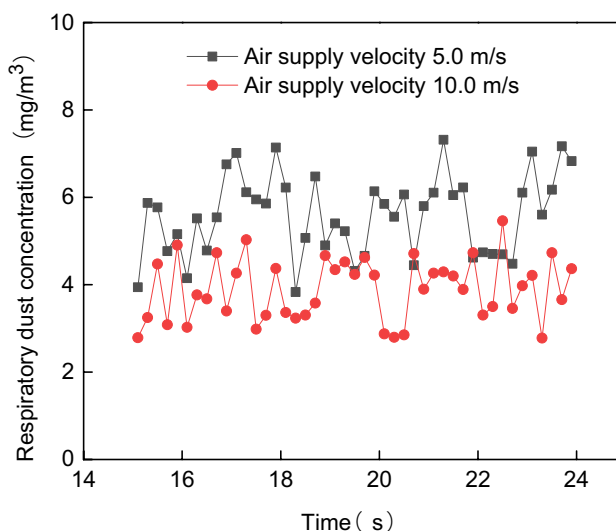


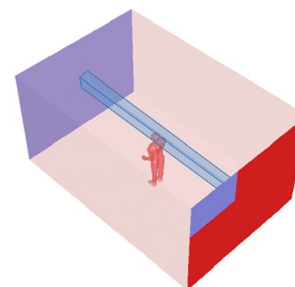
Fig. 15 Respirable dust concentrations in breathing zone under different air supply velocities

Influence of spatial position

When the worker moves along the x -direction in the roadway, the breathing zone passes through a specific area called the breathing band. A simplified breathing band can be obtained by extending a square plane from the dust-producing surface to the wind surface, as shown by the blue area in Fig. 16. The square plane is centered at the center of the breathing zone. It has the same edge length as the breathing zone diameter.

Figure 17 shows the respirable dust concentration variation in the breathing band's x -direction under different working conditions. The dust concentrations in the x -direction vary similarly for all three working conditions. For instance, under the control condition, the respirable dust concentration is 45.0 mg/m^3 at the position where $x < 1.0$ m because it is close to the dust-producing surface. At $x = 1.0$ m, the respirable dust concentration drops sharply to around 5.00 mg/m^3 and stays at this level until $x = 3.0$ m. Probably because the ventilation effect becomes evident within the $x = 1.0$ – 3.0 m space, in which the airflow carries away most dust. From

Fig. 16 Structure of the breathing band



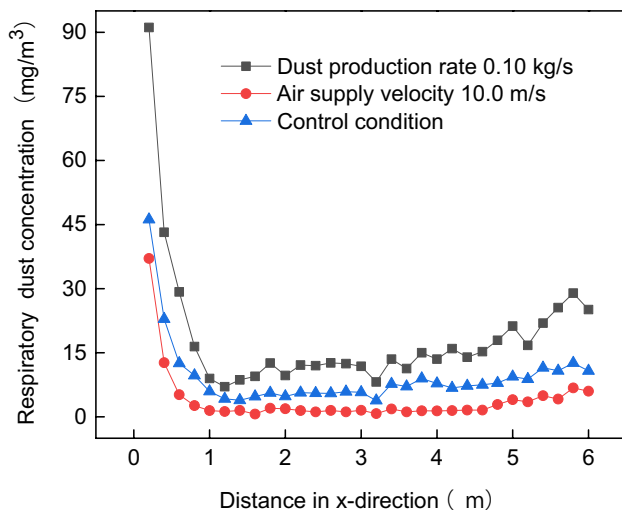


Fig. 17 Respirable dust concentrations in breathing zone under different working conditions

$x = 3.0$ m to the wind surface, the respirable dust concentration decreases first because of the space occupied by the worker's head. It then increases gradually since the dusty airflow near the wind surface slows down and exhibits back mixing due to the negative pressure generated by the high-speed air supply (Fig. 8). Moreover, changing the dust production rate and the air supply velocity alters the overall level of respirable dust rather than the distribution characteristics in the roadway. Under all three working conditions, the higher respirable dust concentrations are found close to the dust-producing and wind surfaces. In comparison, the lower concentrations are found in the middle of the roadway.

Conclusion

This study used the CFD-DPM simulation method to investigate the flow field and respirable dust distribution under a complex underground environment. A Visual Basic program was written to extract and analyze real-time respirable dust concentration data in the breathing zone, which helped to evaluate the dust inhalation for underground coal mine workers. The effects of environmental parameters, such as dust production rate, air supply rate, and spatial location, on dust concentration and distribution were explored. The research results would provide essential data for optimizing ventilation parameters and workers' working principles to reduce dust exposure. The main conclusions are drawn as follows:

(1) The flow field and dust distribution in the breathing zone are mainly influenced by outside airflow and dust characteristics and are rarely affected by human breath.

Therefore, to evaluate the dust inhalation by workers, the outside dust distribution and the human breath can be studied separately instead of considering their complex coupling effects to focus on the real key factors.

(2) Lower dust production rate and higher air supply velocity reduce the respirable dust concentration in the tunnel and the breathing zone of underground workers. Optimizing the ventilation parameters appropriately can effectively reduce workers' potential dust inhalation.

(3) Workers standing in the tunnel would cause complex vortices to affect airflow and dust distribution, which indicates that there would be an optimal working position in the roadway where the respirable dust concentration is relatively lower. In our research, the optimal position was identified to be in the middle of the roadway, more than 1.0 m away from the dust-producing and wind surfaces.

Author contribution All authors contributed to the study's conception and design. Material preparation, data collection, and analysis were performed by Rongting Huang, Wanyi Chen, Yichun Tao, Shilong Yuan, Fan Geng, and Shihang Li. The first draft of the manuscript was written by Rongting Huang and Wanyi Chen. The corresponding author is Rongting Huang. All authors commented on previous versions of the manuscript. All authors read and approved the final manuscript.

Funding This work was supported by the National Natural Science Foundation of China [grant number 52304266]; the Natural Science Foundation of Jiangsu Province [grant number BK20221143]; the Fundamental Research Funds for the Central Universities [grant number 2021QN1087]; and the Double-Innovation Doctor Foundation of Jiangsu Province [grant number JSSCBS20211202].

Data availability We guarantee that data and materials are available.

Declarations

Ethical approval We declare that all authors fully comply with ethical standards.

Consent to participate All agree.

Consent for publication All agree.

Competing interests The authors declare no competing interests.

References

- Alshittawi MS, Suyambazhahan S, Alaboodi AS (2019) Computational fluid dynamics simulation of breathing zone of the human for air quality with a personalized air curtain. *Adv Mech Eng* 11:1–13. <https://doi.org/10.1177/1687814019844688>
- Cai P, Nie W, Chen D-W, Yang S-B, Liu Z-Q (2019) Effect of air flowrate on pollutant dispersion pattern of coal dust particles at fully mechanized mining face based on numerical simulation. *Fuel* 239:623–635. <https://doi.org/10.1016/j.fuel.2018.11.030>

- Chen D, Nie W, Xiu Z-H, Yang B, Du T, Liu Q, Peng H-T (2022) Research on environmental dust pollution: ventilation and dust space-time evolution law of a fully mechanized mining face with 7m mining height. *Environ Sci Pollut Res* 29:33627–33644. <https://doi.org/10.1007/s11356-021-17967-5>
- Chen Z-J, Shi J-Q, Zhang Y, Zhang J-H, Li S-Q, Guan L (2022) Screening of serum biomarkers of coal workers' pneumoconiosis by metabolomics combined with machine learning strategy learning strategy. *Int J Environ Res Public Health* 19:7051. <https://doi.org/10.3390/ijerph19127051>
- Geng F, Luo G, Wang Y-C, Peng Z-B, Hu A-Y, Zhang TT, Chai H-L (2018) Dust dispersion in a coal roadway driven by a hybrid ventilation system: a numerical study. *Process Saf Environ Prot* 113:388–400. <https://doi.org/10.1016/j.psep.2017.11.010>
- Guffey SE, Flanagan ME, Belle G (2001) Air sampling at the chest and ear as representative of the breathing zone. *Am Ind Hyg Assoc J* 62:416–427. <https://doi.org/10.1080/15298660108984643>
- Gui C-G, Geng F, Tang J-H, Niu H-W, Liu C, Teng H-X (2022) Spatial and temporal distribution of dust pollutants from a fully mechanized mining face under the improved air-curtain system. *Adv Powder Technol* 396:467–476. <https://doi.org/10.1016/j.powtec.2021.11.005>
- Gui C-G, Geng F, Tang J-H, Niu H-W, Zhou F-B, Liu C, Hu S, Teng H-X (2020) Gas-solid two-phase flow in an underground mine with an optimized air-curtain system: a numerical study. *Process Saf Environ Prot* 140:137–150. <https://doi.org/10.1016/j.psep.2020.04.028> Get rights and content
- Gupta JK, Lin C-H, Chen Q (2011) Transport of expiratory droplets in an aircraft cabin. *Indoor Air* 21:3–11. <https://doi.org/10.1111/j.1600-0668.2010.00676.x>
- Hu S-Y, Liao Q, Feng G-R, Huang Y-S, Shao H (2020) Influences of ventilation velocity on dust dispersion in coal roadways. *Powder Technol* 360:683–694. <https://doi.org/10.1016/j.powtec.2019.09.080>
- Hu S-Y, Gao Y, Feng G-R, Hu F, Liu C-H, Li J-H (2021) Experimental study of the dust-removal performance of a wet scrubber. *Int J Coal Sci Technol* 8(2):228–239. <https://doi.org/10.1007/s40789-021-00410-y>
- Jiang J-H, Wang P-F, Pei Y, Liu R-H, Liu L-M, He Y-C (2021) Preparation and performance analysis of a coking coal dust suppressant spray. *Int J Coal Sci Technol* 8(5):1003–1014. <https://doi.org/10.1007/s40789-021-00406-8>
- Li S-H, Xie B, Hu S-D, Jin H, Liu H, Tan X-Y, Zhou F-B (2019) Removal of dust produced in the roadway of coal mine using a mining dust filtration system. *Adv Powder Technol* 30:911–919. <https://doi.org/10.1016/j.apt.2019.02.005>
- Lidén G, Waher J (2010) Experimental investigation of the concept of a 'breathing zone' using a mannequin exposed to a point source of inertial/sedimenting particles emitted with momentum. *Ann Occup Hyg* 54:100–116. <https://doi.org/10.1093/annhyg/mep075>
- Liu Q, Nie W, Hua Y, Hua Y, Peng H, Liu C-Q, Wei C-H (2019) Research on tunnel ventilation systems: dust diffusion and pollution behaviour by air curtains based on CFD technology and field measurement. *Build Environ* 147:444–460. <https://doi.org/10.1016/j.buildenv.2018.08.061>
- Lu X-X, Wang C-Y, Xing Y, Shen C, Shi G-Y (2021) Investigation on the dust migration behavior and safety zone in the fully mechanized mining face. *Environ Sci Pollut Res* 28:20375–20392. <https://doi.org/10.1007/s11356-020-12050-x>
- Mo J-M, Yang J-L, Ma W, Chen F, Zhang S-J (2020) Numerical simulation and field experiment study on onboard dust removal technology based on airflow-dust pollution dispersion characteristics. *Environ Sci Pollut Res* 27:1721–1733. <https://doi.org/10.1007/s11356-019-06847-8>
- Ojima J (2012) Gaseous contaminant distribution in the breathing zone. *Ind Health* 50:236–238. <https://doi.org/10.2486/indhealth.MS1314>
- Paluchamy B, Mishra DP, Panigrahi DC (2021) Airborne respirable dust in fully mechanised underground metalliferous mines-generation, health impacts and control measures for cleaner production. *J Clean Prod* 296:126524. <https://doi.org/10.1016/j.jclepro.2021.126524>
- Shekarian Y, Rahimi E, Shekarian N, Rezaee M, Pedram R (2021) An analysis of contributing mining factors in coal workers' pneumoconiosis prevalence in the United States coal mines, 1986–2018. *Int J Coal Sci Technol* 8(6):1227–1237. <https://doi.org/10.1007/s40789-021-00464-y>
- Song S-Z, Zhou G, Duan J-J, Meng Q-Z, Sun B, Wang Y-M (2021) CFD simulation of multi-phase and multi-component diffusion of air-dust-gas in a fully mechanized mining face. *Environ Sci Pollut Res* 28:18260–18275. <https://doi.org/10.1007/s11356-020-11850-5>
- Trechera P, Querol X, Lah R, Johnson D, Wrana A, Williamson B, Moreno T (2022) Chemistry and particle size distribution of respirable coal dust in underground mines in Central Eastern Europe. *Int J Coal Sci Technol* 9(1):3. <https://doi.org/10.1007/s40789-022-00468-2>
- Wang Y, Luo G, Geng F, Li Y-B, Li Y-L (2015) Numerical study on dust movement and dust distribution for hybrid ventilation system in a laneway of coal mine. *J Loss Prev Process Ind* 36:146–157. <https://doi.org/10.1016/j.jlp.2015.06.003>
- Wang H, Nie W, Cheng W-M, Liu Q, Jin H (2018) Effects of air volume ratio parameters on air curtain dust suppression in a rock tunnel's fully-mechanized working face. *Adv Powder Technol* 29:230–244. <https://doi.org/10.1016/j.apt.2017.11.007>
- Xie Z-W, Xiao Y-M, Jiang C-X, Ren Z-L, Li X-Q, Yu K-C (2021) Numerical study on fine dust pollution characteristics under various ventilation time in metro tunnel after blasting. *Build Environ* 204:10811. <https://doi.org/10.1016/j.buildenv.2021.108111>
- Yao H-F, Wang H-Y, Li Y-C, Jin L (2020) Three-dimensional spatial and temporal distributions of dust in roadway tunneling. *Int J Coal Sci Technol* 7:88–96. <https://doi.org/10.1007/s40789-020-00302-7>
- Yin W-J, Zhou G, Gao D-H (2019) Simulation analysis and engineering application of distribution characteristics about multi-stage atomization field for cutting dust in fully mechanized mining face. *Adv Powder Technol* 30:2600–2615. <https://doi.org/10.1016/j.apt.2019.08.007>
- Zhang H, Han W, Xu Y, Wang Z-F (2021) Analysis on the development status of coal mine dust disaster prevention technology in China. *J Healthc Eng* 2021:5574579. <https://doi.org/10.1155/2021/5574579>
- Zhao Z (2023) Research on the motion equation of respirable dust in fully mechanized excavation face. *Min Saf Environ Prot* 50:14–18. <https://doi.org/10.19835/j.issn.1008-4495.2023.01.003>. (in Chinese)
- Zhou G, Kong Y, Meng Q-Z, Jiang B-Y, Liu Y-W, Li G, Sun B, Wang J-L, Yan D, Li Z-H (2022) Research on dust dispersion law of fully mechanized mining faces under different inclinations and tracking closed dust control method. *Sci Rep* 12:16633. <https://doi.org/10.1038/s41598-022-20606-9>
- Zhu J-T, He X-J, Wang L, Liao X-X, Teng G-P, Jing P-L (2022) Performance of N95 elastomeric respirators in high humidity and high coal dust concentration environment. *Int J Min Sci Technol* 32(1):215–224. <https://doi.org/10.1016/j.ijmst.2021.11.007>

Publisher's Note Springer Nature remains neutral with regard to jurisdictional claims in published maps and institutional affiliations.

Springer Nature or its licensor (e.g. a society or other partner) holds exclusive rights to this article under a publishing agreement with the author(s) or other rightsholder(s); author self-archiving of the accepted manuscript version of this article is solely governed by the terms of such publishing agreement and applicable law.